Marine Structures 92 (2023) 103500

Contents lists available at ScienceDirect

Marine Structures

journal homepage: www.elsevier.com/locate/marstruc

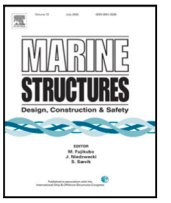

Influence of seabed profile on the seismic response of monopile-supported offshore wind turbines including dynamic soil-structure interaction

Eduardo Rodríguez-Galván *, Guillermo M. Álamo, Cristina Medina, Orlando Maeso

Instituto Universitario de Sistemas Inteligentes y Aplicaciones Numéricas en Ingeniería, Universidad de Las Palmas de Gran Canaria, 35017 Las Palmas de Gran Canaria, Spain

ARTICLE INFO

Keywords:
Offshore wind turbines
Seabed profile
Soil-structure interaction
Kinematic interaction
Monopile
Seismic response

ABSTRACT

In this article, the seismic response of four different Offshore Wind Turbines (OWTs) from 5 to 15 MW, founded on monopiles embedded in homogeneous and non-homogeneous soil profiles with equivalent shear-wave velocities from 100 to 300 m/s is analysed. Two types of variable soil profiles with a semi-parabolic variation of the shear-wave velocity as depth increases are considered. The system seismic response under ten different accelerograms is computed through a finite element substructuring model in frequency domain. The foundation behaviour is obtained by a continuum model including kinematic and inertial interaction. Several models, in addition to that of rigid base condition, are considered to determine the influence of soil-structure interaction (SSI), as well as the contribution of each kinematic interaction (KI) factor. The seismic response of the OWTs is obtained in terms of maximum shear forces and bending moments at mudline level, as well as the acceleration amplification factor at hub level. It is found that the maximum response is produced when SSI is considered, including both the inertial and kinematic interaction. The differences arising due to the soil profile definition are shown to be mainly related to the rotational KI factor, which significantly affects the second vibration mode of the system. The largest responses are obtained for the homogeneous equivalent profile.

1. Introduction

The broad growth experienced by offshore wind energy in recent years has led to considering the installation of offshore wind farms in seismically active regions. As a consequence, the seismic analysis of this type of structures has gone from being a secondary hypothesis to becoming a relevant consideration. In fact, recommended practices are already emerging to reduce seismic risk in wind power plants (such as DNV-RP-0585 "Seismic design of wind power plants" [1], recently published in 2021). In addition, the growing size of wind turbines in search of increasing powers also implies additional uncertainty. Although the influence of the size of wind turbines on their seismic responses has been analysed in previous articles [2,3], such as the one by Medina et al. [2], concluding that the larger the wind turbine, the seismic loads increase to a lesser extent than the environmental loads, the seismic action should not be neglected, since even low or moderate intensity earthquakes can produce significant increases in the structural demands of the Offshore Wind Turbines (OWTs), and a possible combined action (environmental load together with the seismic load) could affect the design of this type of structures, as it is shown by recent works [3–9].

* Corresponding author.
E-mail addresses: eduardo.rodriguezgalvan@ulpgc.es (E. Rodríguez-Galván), guillermo.alamo@ulpgc.es (G.M. Álamo), cristina.medina@ulpgc.es (C. Medina), orlando.maeso@ulpgc.es (O. Maeso).

https://doi.org/10.1016/j.marstruc.2023.103500
Received 5 October 2022; Received in revised form 1 June 2023; Accepted 14 July 2023
Available online 26 July 2023

On the other hand, if wind turbines are founded on deformable soils, the inclusion of the Soil-Structure Interaction (SSI) plays a fundamental role in the dynamic response of the foundation-structure system. The influence of SSI on the dynamic characteristics of OWT has already been addressed in previous articles [10–12], finding all of them relevant variations in the natural frequency due to SSI inclusion, which is a critical factor in the design of this type of structures. Also, in other works [2,13,14] it is demonstrated that the response quantities such as displacements, rotations, accelerations, base shear forces and bending moments are significantly affected by SSI, where its inclusion can double the seismic response with respect to the rigid base assumption, as it is quantified by Medina et al. [2].

The dynamic response of OWTs under seismic loads have been carried out by employing different methodologies. Most of them are based on assuming either a non-linear or linear behaviour for modelling the soil–pile system, and the finite element method to reproduce the superstructure response. The non-linear SSI behaviour is commonly used [4,6–9,11,13,15–19], because it can simulate the plastic and cyclic behaviour of the SSI. In these models the pile–soil interaction is generally reproduced by using non-linear Winkler p-y, t-z and q-z springs, coupled with other finite element programs or codes (such as FAST, OpenSees or Abaqus). In these models, the expressions recommended by the API [20] are commonly used to define the non-linear soil–structure interaction. Nevertheless, these API expressions present significant limitations, since they can only accurately reproduce the pile–soil behaviour of small diameter piles. Besides, another disadvantage of the non-linear assumption is that it requires considerable computational effort. Regarding the linear assumption, it has also been used in numerous works [2,3,21]. Despite being simplified models, they are generally accepted as an initial approach, and they are useful when parametric studies involving a large number of simulations are made. In these linear models, the SSI is usually reduced to a set of impedance functions to reproduce the stiffness and damping of the foundation-soil system, and kinematic interaction factors to represent the filtering of the ground motion produced by the foundation. The linear assumption also allows to study the system response through the frequency domain method (like is made in [2,21]), useful to analyse systems with frequency-dependent and hysteretic damping properties.

Among all the existing types of foundations for offshore wind turbines, the vast majority of them (81.4% in Europe, according to Wind Europe [22]), consist of monopiles. This type of foundation is preferable mainly due to its wide range of installation depths, its low manufacturing cost and ease of installation compared with other foundation types. Monopiles consist of tubular steel sections of large diameters and lengths. Due to their geometric particularities, when monopiles are subjected to seismic excitations they undergo a remarkable rotation, which causes displacements and loads to be taken into account in the wind turbine design. The importance of considering kinematic interaction (KI) in SSI has already been studied by Kaynia [21], showing that such inclusion implies larger responses for a 5 MW wind turbine in different types of soil profiles.

All the works mentioned and those existing in the scientific literature are either carried out on the same type of soil profile or on a single OWT with small rated power (less than or equal to 5 MW). Furthermore, although many seismic SSI analyses can be found [2,3,11,13,14], very few have focused on analysing the KI effects within SSI. For these reasons, this paper aims to study the influence that the type of soil profile has on the seismic response of four OWTs supported by monopiles, analysing for each type of profile the relevance of the inclusion of the inertial and kinematic interaction in the seismic response. For that purpose, three different soil profiles are considered, one homogeneous and two non-homogeneous, the latter two with a semi-parabolic variation of the shear-wave velocity as depth increases. First, the dynamic behaviour of a foundation for a 10 MW OWT embedded in three types of soil profiles, with an equivalent time-average shear-wave velocity for the upper 30 m depth ($V_{S,30}$) of 200 m/s, is analysed in terms of impedances and KI factors. Then, the maximum seismic response of four OWTs from 5 to 15 MW founded on three types of soil profiles is computed. This maximum response is studied assuming various $V_{S,30}$ from 100 to 300 m/s, to consider different soil stiffnesses (soft-to-medium seabeds), and defining various models that allow quantifying the relevance of the inertial and kinematic interaction effects. Finally, to better quantify the relevance of considering the non-homogeneity of the seabed profile, results obtained in all the considered soil profiles and models are compared, addressing the relative differences with respect to the results corresponding to the equivalent homogeneous soil profile.

2. Methodology

The system seismic response is computed through a previously developed finite element substructuring model in the frequency domain [2], where the tower and the substructure are divided into Bernoulli's beam finite elements (see Fig. 1). The flexibility and damping of the foundation-soil are represented by impedances functions for the lateral (or horizontal), rocking and cross-coupled horizontal-rocking vibration modes (denoted as K_H, K_R and K_{HR} in Fig. 1). The filtering of the soil movement by the foundation is represented by lateral (or translational) and rotational KI factors (denoted as I_u and I_θ in Fig. 1). These impedances and KI factors are obtained through a continuum model [23] based on the integral expression of the reciprocity theorem, specially developed to efficiently analyse the harmonic behaviour of pile foundations in layered soils. The use of the substructuring approach allows to separately analyse the contribution of each component of the soil-interaction phenomena, i.e. foundation flexibility and lateral and rotational kinematic interaction, to the system seismic response.

Once the system response is computed in the frequency domain, the response in the time domain is obtained using the frequency domain method [24]. The seismic excitation is assumed to be a planar S wave vertically propagating through the soil, producing a free-field (without foundation) lateral displacement at ground level denoted as u_{ff} in Fig. 1. In order to isolate the seismic response, no environmental loads due to wind or waves are considered in this study.

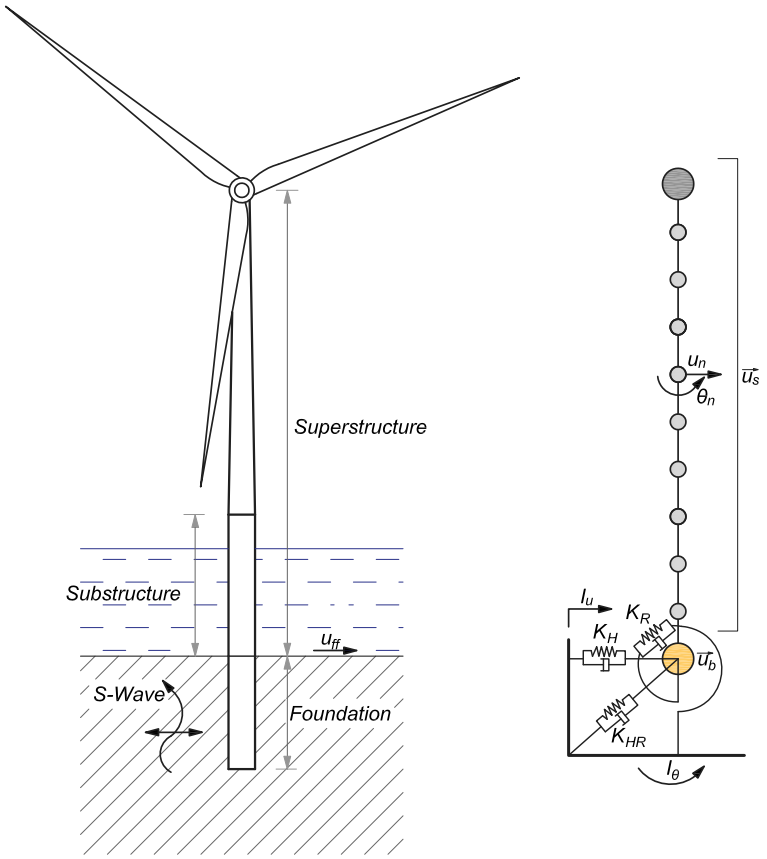

Fig. 1. Substructuring model used in this work.
Source: Adapted from: [2].

2.1. Superstructure modelling

Given the particularities of the problem, only the lateral behaviour of the structure is taken into account. The wind turbine hollow tower and the monopile are divided into finite elements of two nodes (Bernoulli's beams). Based on a convergence study, a sufficiently large number of elements is used, so that the conical shape of the tower is reproduced accurately enough. In this way, each node has two degrees of freedom: a lateral displacement (u_n) and a rotation (θ_n). Distributed inertial properties are assumed for each element. A hysteretic damping model is used for the steel of the monopile and the tower. The stiffness and elementary mass matrices used for each element are shown in Eqs. (1) and (2), being L_e the element length, A_e the cross-sectional area of the element, I_e the moment of inertia of the section area, ρ the material density and E^* the Young's Modulus of the material, including the hysteretic damping ($E^* = E(1+2i\xi)$, being ξ the hysteretic damping ratio and i the imaginary unit). These matrices are assembled to obtain the overall stiffness and mass matrix. The mass of the rotor-nacelle assembly is considered as a punctual mass at the top node. For simplification reasons, the transition piece between the monopile and the tower is not considered.

$$K_e^* = \frac{E^* I_e}{L_e^3}\begin{bmatrix} 12 & 6L_e & -12 & 6L_e \\ 6L_e & 4L_e^2 & -6L_e & 2L_e^2 \\ -12 & -6L_e & 12 & -6L_e \\ 6L_e & 2L_e^2 & -6L_e & 4{L_e}^2 \end{bmatrix} \tag{1}$$

$$M_e = \frac{\rho A_e L_e}{420}\begin{bmatrix} 156 & 22L_e & 54 & -13L_e \\ 22L_e & 4L_e^2 & 13L_e & -3L_e^2 \\ 54 & 13L_e & 156 & -22L_e \\ -13L_e & -3L_e^2 & -22L_e & 4{L_e}^2 \end{bmatrix} \tag{2}$$

2.2. Foundation modelling

The interaction of the structure with the foundation is modelled through the foundation impedance matrix (K_{SSI}), which represents the stiffness and damping of the monopile under the mudline level. As shown in Eq. (3), this matrix is made up of a

horizontal or lateral (K_H), a rocking (K_R) and a cross-coupled (K_{RH} and K_{HR}) impedance functions. All these terms represent the force or moment that should be applied at the monopile head to achieve an unitary displacement or rotation in each of its degrees of freedom, while restricting the rest. These are complex-valued, frequency dependent terms, whose real and imaginary parts represent, respectively, the soil-foundation stiffness and damping (energy dissipation).

$$K_{SSI}(\omega) = \begin{bmatrix} K_H(\omega) & K_{HR}(\omega) \\ K_{RH}(\omega) & K_R(\omega) \end{bmatrix} \tag{3}$$

The filtering effect due to the presence of the foundation is considered through the lateral (I_u) and rotational (I_θ) KI factors, which are grouped in a vector $\vec{I}_{SSI}$:

$$\vec{I}_{SSI}(\omega) = \begin{Bmatrix} I_u(\omega) \\ I_\theta(\omega) \end{Bmatrix} \tag{4}$$

both terms are also complex-valued, dependent on the excitation frequency and represent the offset with respect to the displacement that would occur at the mudline level if the foundation did not exist. Therefore, both terms are obtained as the ratio between the pile head displacement or rotation with respect to the free-field motion:

$$I_u(\omega) = \frac{u_p(\omega)}{u_{ff}} \tag{5}$$

$$I_\theta(\omega) = \frac{\theta_p(\omega)}{u_{ff}} \tag{6}$$

The foundation dynamic response in terms of impedances and KI factors is computed through a previously developed continuum numerical model [23]. This model is based on the integral expression of the reciprocity theorem in elastodynamics and the use of advanced fundamental solutions for reproducing the behaviour of the layered soil, which already satisfy the free-field and inter-layer boundary conditions. On the other hand, piles are treated as load lines in the soil formulation and their stiffness and inertial contribution is considered through their definition as beam finite elements. Pile–soil coupling is made by imposing equilibrium and compatibility conditions in terms of displacements and soil–pile interaction forces. Linear-elastic behaviour of soil and piles is assumed. The ability of this model to accurately reproduce the dynamic behaviour of OWT's foundation elements has been demonstrated in [25].

2.3. Coupled system response

Once the mass and stiffness matrices of the superstructure and the foundation behaviour have been obtained, the system of linear equations to be solved to obtain the response of the superstructure in the frequency domain, including the SSI, can be written as:

$$\left(\begin{bmatrix} K^*_{ss} & K^*_{sb} \\ K^*_{bs} & K^*_{bb} + K_{SSI}(\omega) \end{bmatrix} - \omega^2 \begin{bmatrix} M_{ss} & M_{sb} \\ M_{bs} & M_{bb} \end{bmatrix} \right) \begin{Bmatrix} \vec{u}_s(\omega) \\ \vec{u}_b(\omega) \end{Bmatrix} = \begin{Bmatrix} \vec{0} \\ \vec{f}_{SSI}(\omega) \end{Bmatrix} \tag{7}$$

where the subscript b refers to the submatrices corresponding to the base, while the subscript s refers to the rest of the structure. The vector $\vec{u}_s$ corresponds to the displacements and rotations of the active degrees of freedom of the system, while the vector $\vec{u}_b$ represents the displacement and rotation at the superstructure base and pile head connection (mudline level). The vector $\vec{f}_{SSI}$ contains the shear force and the bending moment at the superstructure base node due to soil-foundation interaction, which, in this case, would coincide with the shear force and the moment at the monopile head (see Fig. 1, where it can be seen that below this node there are no more contiguous elements). This vector $\vec{f}_{SSI}$ is calculated as:

$$\vec{f}_{SSI}(\omega) = K_{SSI}(\omega)\vec{I}_{SSI}(\omega) \tag{8}$$

In order to clarify the influence of including inertial and kinematic interaction, five models are defined:

- **Flexible base models: "with KI", "without KI", "I_u contribution" and "I_θ contribution"**
  Results corresponding to flexible base models are computed from Eq. (7), obtaining $\vec{I}_{SSI}$ from Eqs. (4), (9), (10), (11), to include KI factors, both and none of them, only lateral (I_u) or rotational (I_θ) KI factors, respectively. The models that only include the lateral or rotational KI factors (designated as "I_u contribution" and "I_θ contribution"), aim to quantify the contribution of each KI factor separately.

$$\vec{I}_{SSI}(\omega) = \begin{Bmatrix} 1 \\ 0 \end{Bmatrix} \tag{9}$$

$$\vec{I}_{SSI}(\omega) = \begin{Bmatrix} I_u(\omega) \\ 0 \end{Bmatrix} \tag{10}$$

$$\vec{I}_{SSI}(\omega) = \begin{Bmatrix} 0 \\ I_\theta(\omega) \end{Bmatrix} \tag{11}$$

Table 1
Main characteristics of the OWTs used in this work.
Source: [2].

OWT	5 MW [27]	8 MW [28]	10 MW [29]	15 MW [30]
Rotor-Nacelle-Assembly mass (t)	350	480	674	1017
Tower height (m)	90	110	119	135
Rotor diameter (m)	126	164	178.3	240
Rated wind speed (m/s)	11.4	12.5	11.4	10.59
Cut-out wind speed (m/s)	25	25	25	25
Rotor operational speed range (rpm)	6.9–12.1	6.3–10.5	6–9.6	5–7.56
Tower top diameter (m)	3.87	5	5.5	6.5
Tower bottom diameter (m)	6	7.7	8.3	10
Tower top thickness (m)	0.019	0.022	0.020	0.024
Tower bottom thickness (m)	0.027	0.036	0.038	0.041
Pile diameter (m)	6.04	7.70	8.30	10.00
Pile thickness (m)	0.067	0.084	0.090	0.107
Pile length over mudline (m)	32.6	32.6	32.6	32.6
Pile embedded length (m)	49.7	60.1	63.8	73.8

- **Rigid base model**
  The rigid base assumption implies neglecting SSI effects. Thus, the structure is subjected to the free-field motion directly at its base. Therefore, results for this scenario can be obtained as:

$$(K_{ss}^{*} - \omega^2 M_{ss})\vec{u}_s(\omega) = -(K_{sb}^{*} - \omega^2 M_{sb}) \begin{Bmatrix} 1 \\ 0 \end{Bmatrix} \tag{12}$$

Once the system displacements and rotations are obtained, the nodal values of the internal forces ($\vec{f}_e$, shear forces V and bending moments M) of each element e can be directly computed through:

$$\vec{f}_e = (K_e^{*} - \omega^2 M_e)\vec{u}_e \tag{13}$$

The calculated displacements, rotations and internal forces constitute the system's frequency response functions (FRFs) with respect to the free-field motion. Then, using the frequency domain method [24], the results in the time domain are obtained. Finally, the maximum value of the time history of internal forces and accelerations that take place in the entire system are computed. As shown in Medina et al. [2], the maximum shear forces and bending moments of the superstructure are reached at the mudline level, while the maximum accelerations occur at the nacelle height. Therefore, these are the variables studied in this article to quantify the system seismic response.

3. Problem definition

3.1. OWT properties

The four reference OWTs (see Table 1) as well as the corresponding monopiles (also shown in Table 1) considered in this study are extracted from Medina et al. [2], where monopiles sizing is addressed based on the procedure described by Arany et al. [26].

Both the wind turbine tower and the monopile are considered of S355 structural steel, whose main characteristics are: Young's modulus of 210 GPa, Poisson's ratio of 0.3 and density of 7850 kg/m^3. A hysteretic damping coefficient of 2% is considered for this steel.

3.2. Soil properties

Three types of soil profiles are studied in this article: a homogeneous profile and two non-homogeneous profiles (depth-dependent shear-wave velocity). Equivalent time-average shear-wave velocities for the upper 30 m depth ($V_{S,30}$) between 100 and 300 m/s (with steps of 25 m/s), representing different soft-to-medium seabeds, are used for each type of soil profile. The rest of seabed properties are considered constant with depth for all the soils. In this way, a Poisson's ratio of 0.49, a density of 2000 kg/m^3 and a hysteretic damping of 2.5% are adopted. These are typical values of moderately saturated sands.

To define the two variable profiles, one of the expressions treated by Wang and Wang [31], previously proposed by Hamilton [32], has been used. It defines a simple power law model, as shown in Eq. (14), where the parameter A represents the scale of the shear-wave velocity, and the exponent n indicates the increase in speed with depth.

$$V_S(z) = Az^n \tag{14}$$

Wang and Wang [31] compute A and n by fitting data from real soil wells from California and Japan, obtaining exponent values n between approximately 0.2 and 0.5. The boreholes treated by Wang and Wang include a wide variety of soils, being their results representative of other seismically active regions, e.g the Mediterranean area. In order to cover this range, non-homogeneous seabed

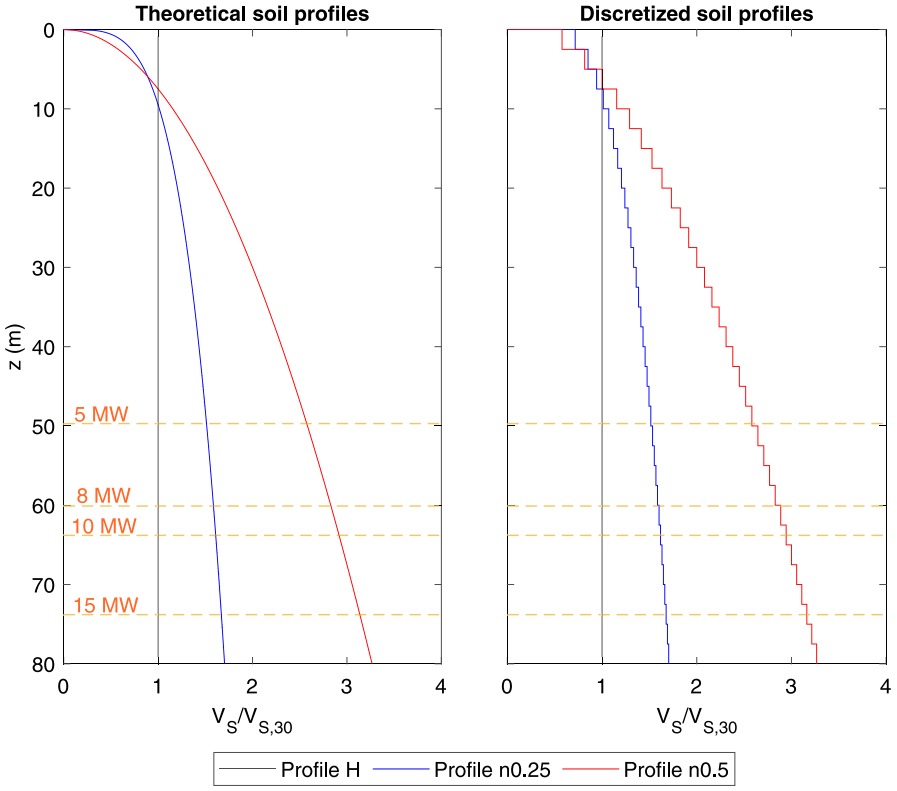

Fig. 2. Theoretical soil profiles studied (left) and discretized soil profiles (right).

Table 2
Information about the seismic signals (accelerograms) used in this work.
Source: [34].

RSN	Dir.(º)	Event Name	Year	Station Name	$V_{S,30}$ (m/s)	$a_{g,max}$ (g)
186	90	Imperial Valley-06	1979	Niland Fire Station	212	0.11
266	102	Victoria Mexico	1980	Chihuahua	242	0.15
729	0	Superstition Hills-02	1987	Imperial Valley W.L.A	179	0.21
1176	60	Kocaeli Turkey	1999	Yarimca	297	0.23
1498	59	Chi-Chi Taiwan	1999	TCU059	273	0.16
1792	90	Hector Mine	1999	Indio-Riverside C.F.G	282	0.12
2715	47	Chi-Chi Taiwan-04	1999	CHY047	170	0.13
3683	11	Taiwan SMART1(45)	1986	SMART1 O11	295	0.13
3965	8	Tottori Japan	2000	TTR008	139	0.32
5666	7	Iwate Japan	2008	MYG007	167	0.13

profiles with $n = 0.25$ and 0.5 are considered in this study. The scale parameter (A) is calculated by replacing Eq. (14) in Eq. (15), established in Eurocode 8 [33], in order to obtain different profiles with the same average shear-wave velocity.

$$V_{S,30} = \frac{30}{\int_0^{30} \frac{dz}{V_S(z)}} \tag{15}$$

Thus, the considered non-homogeneous soil profiles are defined by Eq. (16):

$$V_S(z) = \frac{V_{S,30}}{30^n(1-n)} z^n \tag{16}$$

Fig. 2 shows the variation with depth of shear-wave velocity for the homogeneous soil (named "Profile H" and represented by a black line) and variable soil profiles with $n = 0.25$ ("Profile n0.25", blue line) and $n = 0.5$ ("Profile n0.5", red line). Dashed horizontal lines represent the monopile embedded length for each OWT. To model the non-homogeneous profiles, the soil is discretized into homogeneous layers of 2.5 m deep. The resulting profile of shear-wave velocities throughout the entire depth of the soil is displayed in Fig. 2 right graph.

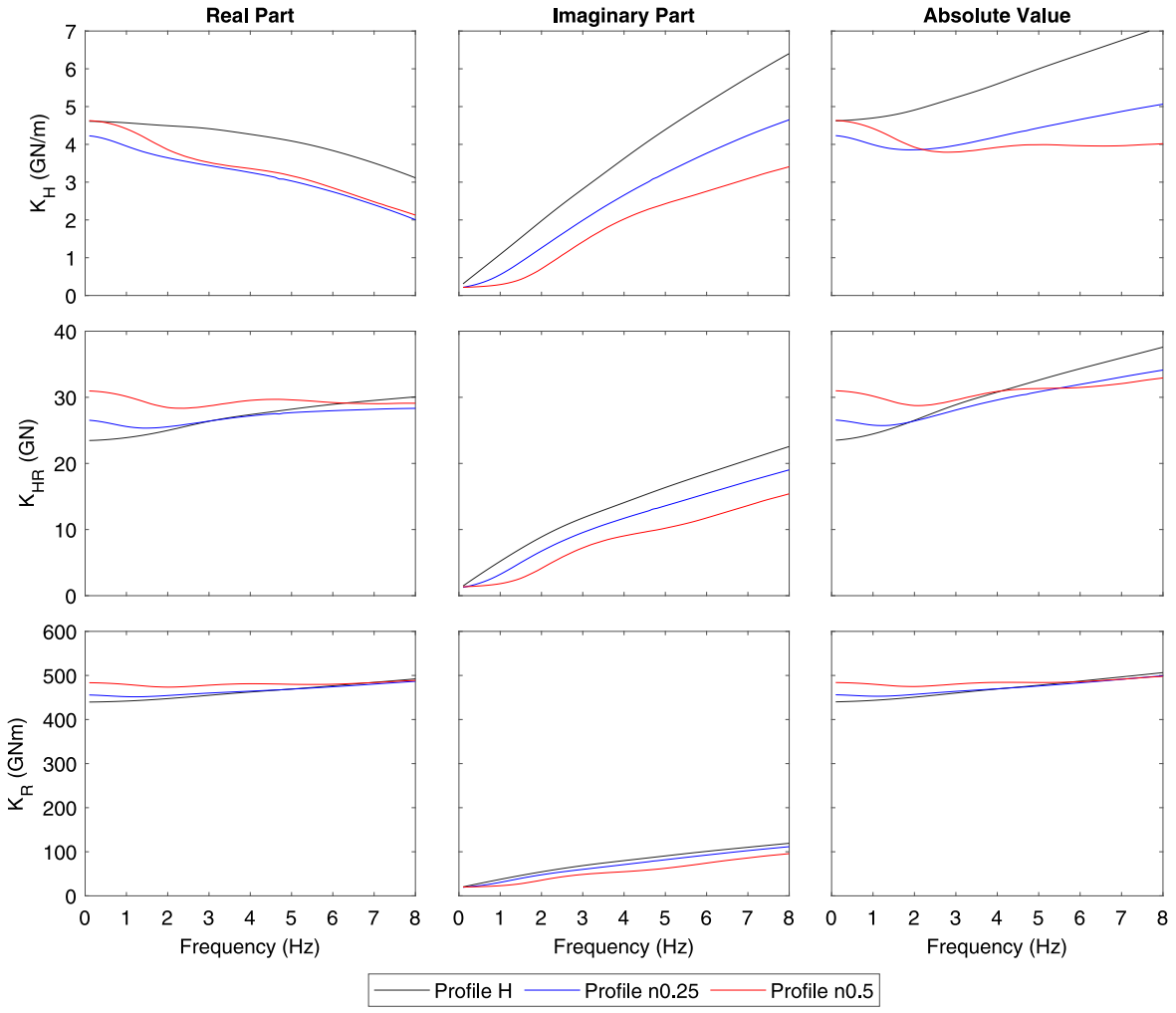

Fig. 3. Impedances functions for the three soil profiles with $V_{S,30} = 200$ m/s and the 10 MW OWT.

Table 3
Modal frequencies of the 10 MW OWT in all soils.

	$V_{S,30}$ (m/s)	100	125	150	175	200	225	250	275	300
Profile H	1st **mode (Hz)**	0.205	0.207	0.209	0.210	0.211	0.212	0.213	0.213	0.213
	2nd **mode (Hz)**	1.420	1.470	1.507	1.535	1.557	1.574	1.587	1.598	1.607
Profile n0.25	1st **mode (Hz)**	0.203	0.206	0.207	0.209	0.210	0.210	0.211	0.212	0.212
	2nd **mode (Hz)**	1.370	1.424	1.465	1.496	1.520	1.539	1.555	1.568	1.579
Profile n0.5	1st **mode (Hz)**	0.203	0.205	0.207	0.208	0.209	0.210	0.210	0.211	0.211
	2nd **mode (Hz)**	1.364	1.415	1.454	1.483	1.505	1.523	1.538	1.551	1.561

3.3. Seismic signals

The ten accelerograms used in Medina et al. [2], all of them obtained from the PEER Ground Motion Database [34] are also considered in this work. These earthquakes have been measured in soils with $V_{S,30}$ values between 100 and 300 m/s, covering the same range of $V_{S,30}$ established for the soil profiles used in this study. Table 2 provides the main information of each earthquake: the record sequence number (RSN) of the database, the direction with respect to the north of the horizontal component used, name and year of the earthquake event, name of the measuring station, the $V_{S,30}$ of the soils in which they were measured and the maximum ground acceleration ($a_{g,max}$) of the signal.

In order to make the results obtained for each earthquake comparable to each other, once the system response for each seismic signal is calculated, it is divided by the maximum ground acceleration of each signal. Finally, the average response of the ten

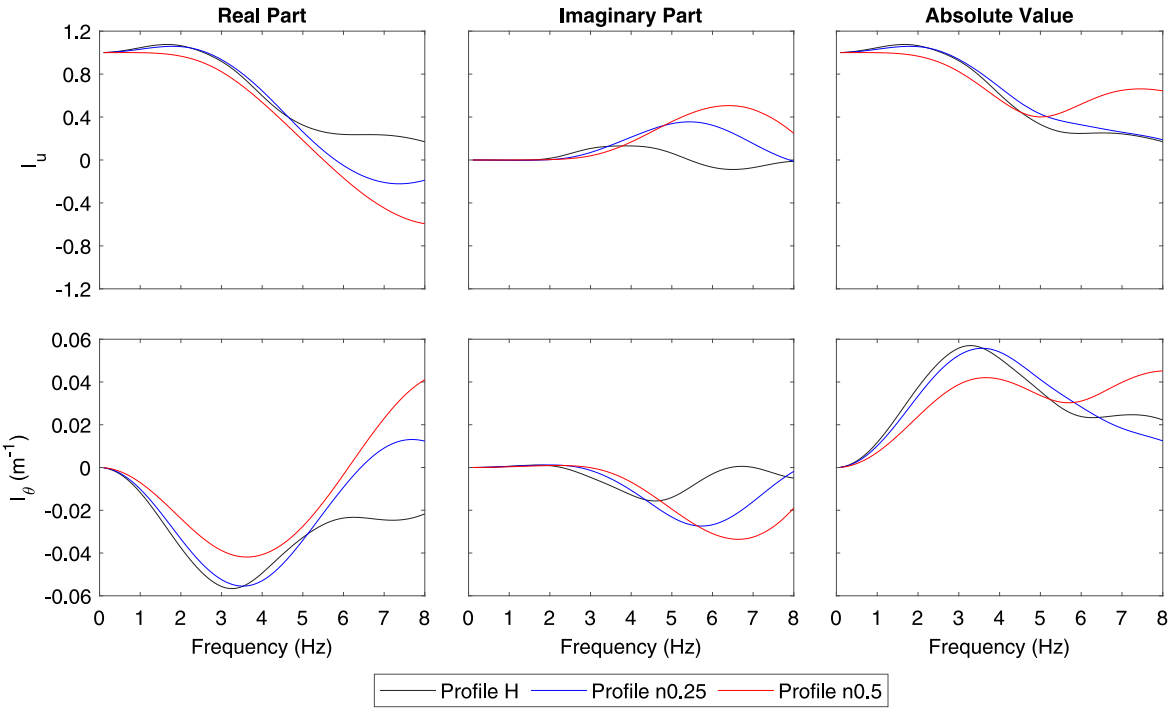

Fig. 4. KI factors for the three soil profiles with $V_{S,30} = 200$ m/s and the 10 MW OWT.

accelerograms is analysed, following the guidelines of DNV-RP-0585 [1], where it is recommended to use the mean response of, at least, seven earthquakes.

4. Results

This section is organized as follows: first, the foundation behaviour of the 10 MW OWT founded on the three types of soil profiles with a $V_{S,30} = 200$ m/s is studied as a representative configuration. The frequency dependence and the influence of the soil profile on the foundation-soil impedances (Fig. 3) and KI factors (Fig. 4) is analysed. Secondly, the first two modal frequencies of this OWT in all soils considered are studied (Table 3), in order to quantify the variation of the natural frequencies of the system depending on the soil profile on which it is founded. Then, the foundation behaviour for the first and second vibration mode of the system is studied, also in terms of impedances and KI factors (Figs. 5 and 6 respectively). After the analysis of the foundation behaviour, the maximum scaled seismic response in terms of amplification factors (Fig. 7), shear forces (Fig. 8) and bending moments (Fig. 9) is presented, comparing the contribution of the inertial and kinematic interaction. Finally, the effect of considering a homogeneous or non-homogeneous soil profile is examined. This influence is quantified in terms of relative differences between the maximum results computed in the two variable with depth soil profiles with respect to those of the homogeneous profile, also in terms of amplification factors, shear forces and bending moments (Figs. 10, 11 and 12 respectively).

4.1. Foundation behaviour

Fig. 3 shows the lateral K_H (first row), cross-coupled K_{HR} (second row) and rocking K_R (third row) impedances computed for the monopile of the 10 MW OWT founded on the three types of soil profiles with $V_{S,30} = 200$ m/s. The different columns present the real part (stiffness component), imaginary part (damping component) and absolute value of the impedance functions. Frequency is represented in the horizontal axis, where a frequency range from 0 to 8 Hz is considered, as a result of a convergence study. Results for homogeneous (black line), and variable profiles with $n = 0.25$ (blue line) and 0.5 (red line) are presented in a superimposed manner. Comparing the stiffness components, i.e. real parts, it can be seen that lateral impedances for the homogeneous profile are greater than those obtained for non-homogeneous profiles throughout the considered frequency range. The opposite occurs with cross-coupled and rocking impedances, which reach higher values for variable soil profiles, at least up to a frequency of 4–5 Hz. Note also that the highest rocking and cross-coupled impedances are obtained for the soil profile with the more pronounced variation of shear-wave velocity with depth. This trend (agreeing with the findings of previous works [35–37]) is due to the fact that the cross-coupled and rocking impedances are more affected by ground stiffness in the deeper layers, while the lateral impedance is more influenced by the layers near to the mudline level or seabed surface. Notice how in Fig. 2 this is appreciable, the two variable soils are stiffer in deep layers, while the homogeneous soil is stiffer in upper layers. Furthermore, it can also be seen that the rocking

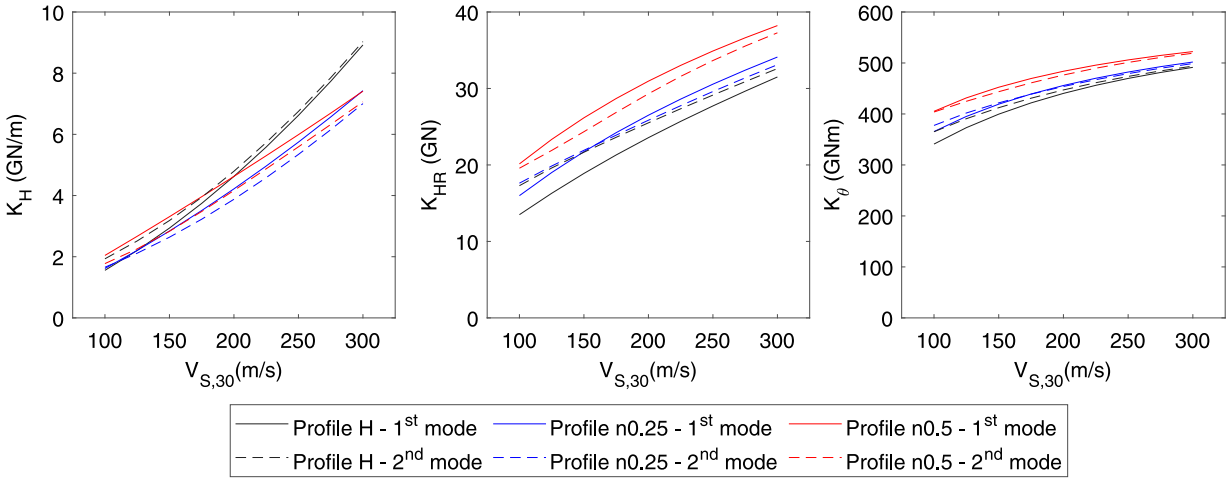

Fig. 5. Impedances vs $V_{S,30}$ in the first and second vibration mode for the 10 MW OWT.

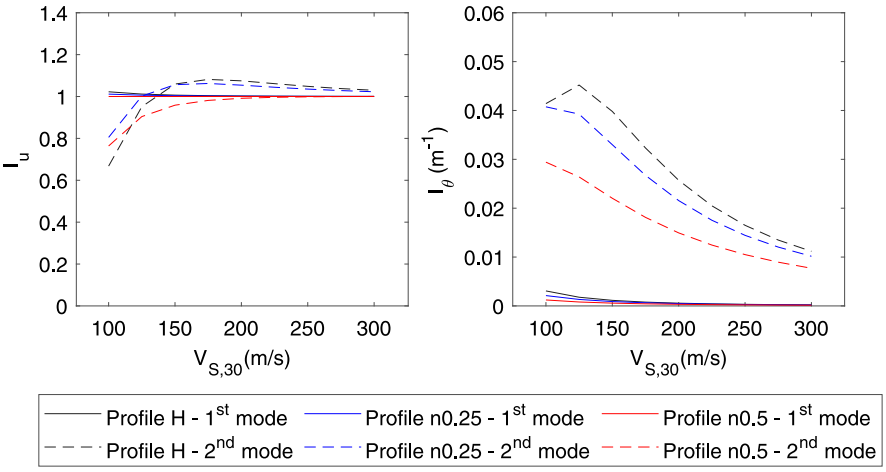

Fig. 6. KI factors vs $V_{S,30}$ in the first and second vibration mode for the 10 MW OWT.

impedances for the homogeneous and non-homogeneous with $n = 0.25$ profiles are quite similar to each other in comparison with those of the non-homogeneous profile with $n = 0.5$, which is much stiffer in the deeper layers than the other two profiles (see Fig. 2). Regarding the imaginary parts, the foundation damping increases with higher frequencies for the three soil profiles, which is typical of the radiation effects. In all vibration modes, the imaginary parts of the homogeneous profile are the greatest, followed by those of the non-homogeneous profile with $n = 0.25$. The absolute value of the impedance functions presents a similar trend that the one of stiffness component, slightly increasing its value at higher frequency due to the contribution of the damping.

In the same way, following the same graphic distribution as the one used in Figs. 3, 4 shows the results obtained in terms of KI factors in the frequency range considered, also for the 10 MW OWT and for a $V_{S,30} = 200$ m/s. The lateral KI factor (I_u) is shown in the first row and the rotational KI factor (I_θ) in the second one. The absolute value of the KI factors represents the filtering effect of the foundation. It shows that the lateral KI factors are quite similar for the three types of soil profiles (at least up to a frequency between 4 and 5 Hz). Regarding the rotational KI factor, a greater difference is observed between the three types of seabed profiles considered. Generally, the rotational KI factor for the homogeneous soil and for the non-homogeneous soil with $n = 0.25$ are similar, unlike those obtained for the variable soil with $n = 0.5$, which show considerable differences with respect to the other two soil profiles, obtaining a lower rotation in this latter profile (at least up to a frequency of 5 Hz). Analysing the real and imaginary parts of the KI factors, it can be observed that, for frequencies smaller than 2 Hz, the foundation and soil movement are both in phase (for these frequencies the rotational and lateral kinematic interaction factors are real valued). For frequencies larger than 2 Hz, foundation and soil movements become out of phase.

In order to study the influence of $V_{S,30}$ on the foundation behaviour for each type of seabed profile, the impedances and KI factors corresponding to the first two modes of vibration of the 10 MW OWT are analysed. To do this, the first two vibration modes are identified in each seabed considering the SSI. Table 3 shows these natural frequencies for each $V_{S,30}$. As can be seen, the more

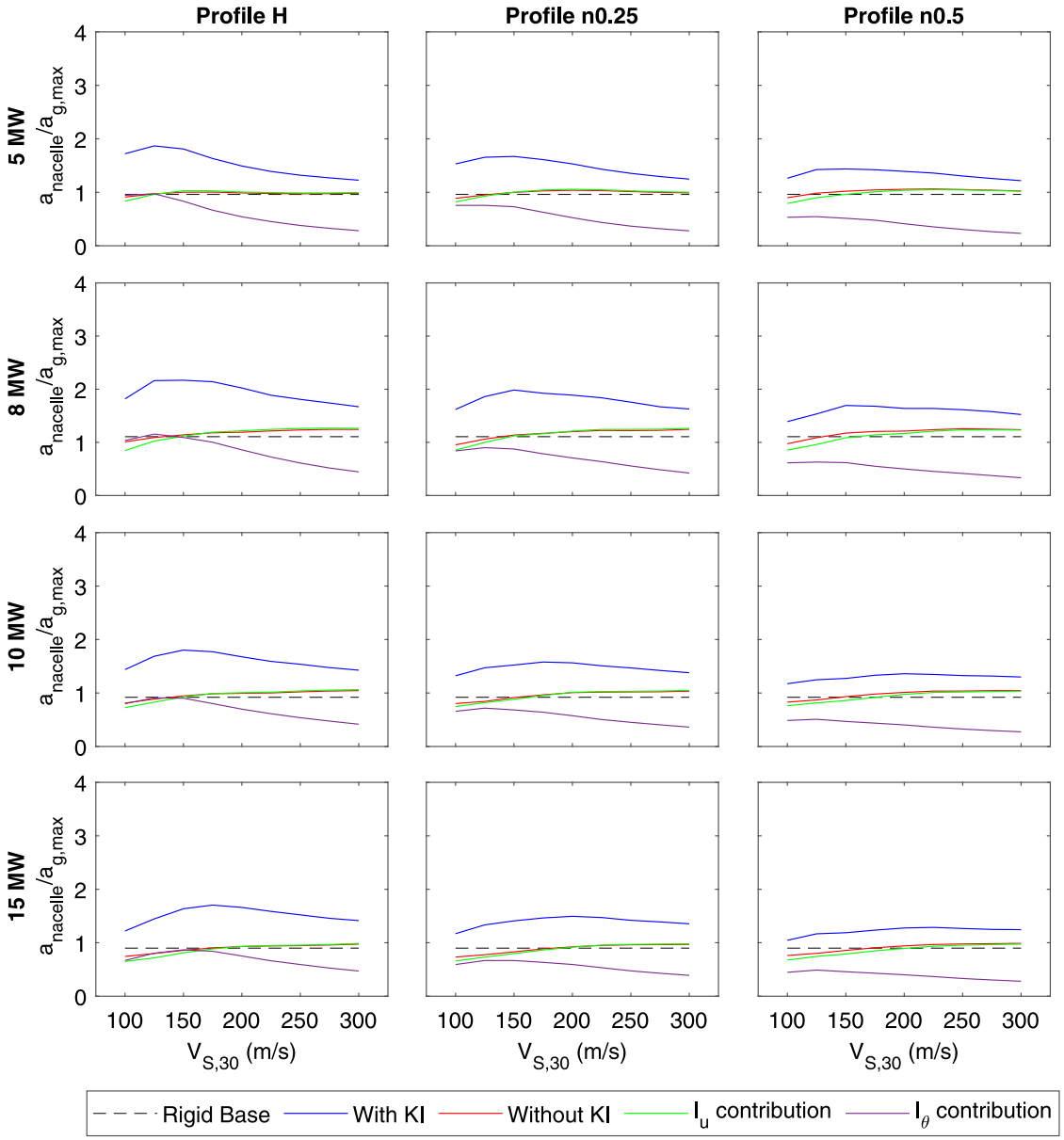

Fig. 7. Amplification factors at the nacelle height vs $V_{S,30}$ for all the study cases.

pronounced the variation of shear-wave velocity with depth, the lower the natural frequency. So, the system natural frequencies are also highly influenced by the layers closest to the mudline level. Note that when considering homogeneous soil (stiffer in upper layers), the largest natural frequencies are obtained. On the other hand, the modal shapes are not significantly affected by the soil profile.

Fig. 5 shows the impedances obtained for the first and second modes against $V_{S,30}$. The lateral, cross-coupled and rocking impedances are represented in the first, second and third column respectively. Results corresponding to the first mode are indicated by continuous lines, while those corresponding to the second mode are represented by dashed lines. For simplification reasons, only the absolute value is shown. Results for different seabed profiles are displayed with the same colours used in previous figures. It can be seen that as ground stiffness increases (crescent $V_{S,30}$), higher impedances are obtained both for the first and the second mode. In addition, in the homogeneous soil, larger impedances are obtained for the second mode in comparison with those corresponding to the first mode. The opposite occurs in the non-homogeneous profile with more pronounced variation of V_S ($n = 0.5$), where impedances corresponding to the second mode are slightly smaller than those for the first mode. While in the non-homogeneous profile with less pronounced variation of V_S ($n = 0.25$), similar impedances are reached for the two vibration modes. In general, the trend of the results in the two vibration modes is quite similar to what has been previously commented: the more pronounced is the

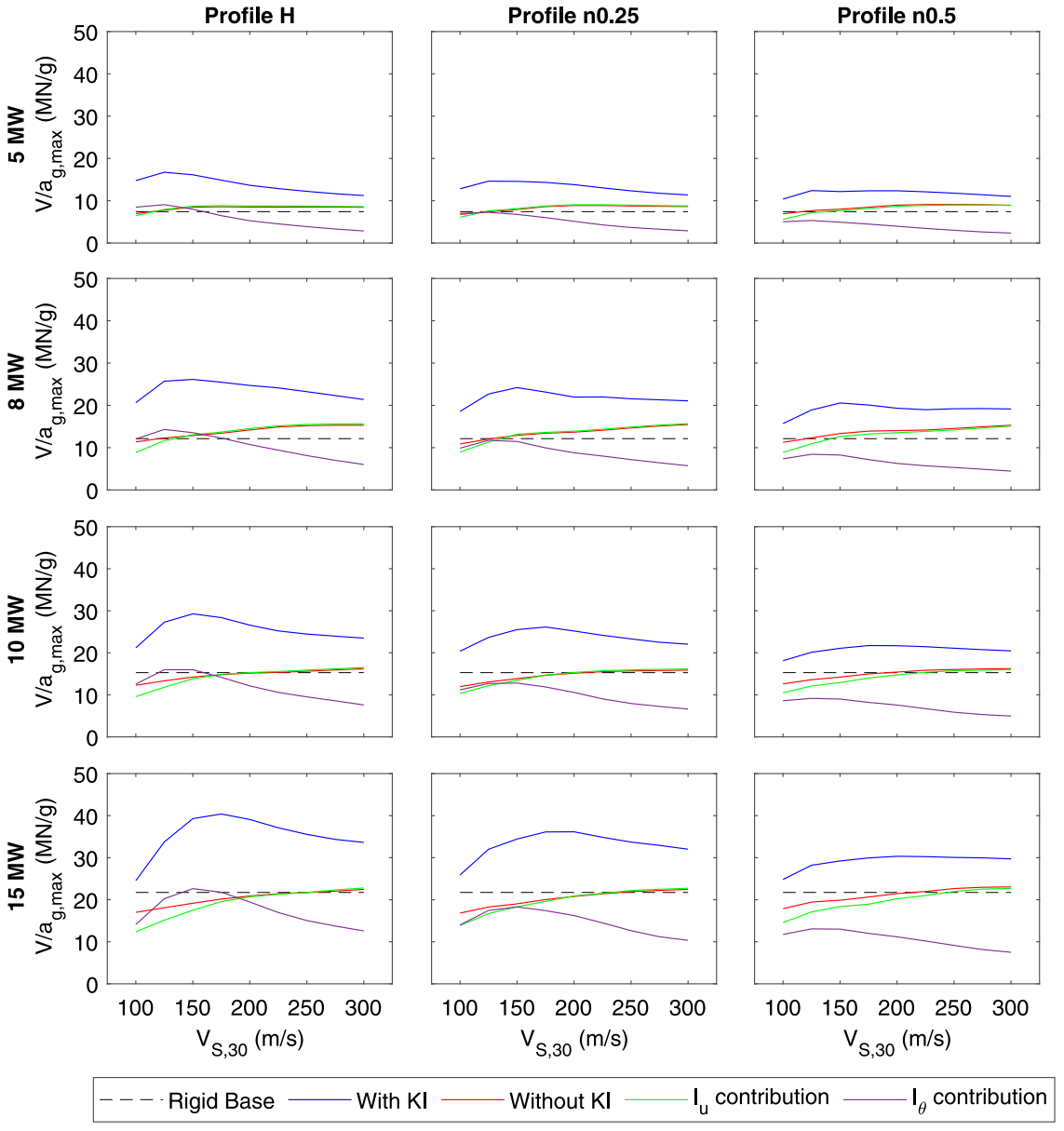

Fig. 8. Shear forces at the mudline level vs $V_{S,30}$ for all the study cases.

variation of V_S with depth in the soil profile, the greater the rocking and cross-coupled impedances are for all the values considered for $V_{S,30}$; while in the homogeneous soil the lateral impedances are bigger for $V_{S,30}$ greater than 200 m/s in the first mode, and for all the $V_{S,30}$ range in the second mode. Also, in the second mode and for all the $V_{S,30}$ range, it can be seen that the rocking and cross-coupled impedances obtained in the homogeneous and non-homogeneous profile with $n = 0.25$ are very similar to each other.

The KI factors (absolute values) for the first two modes against the different $V_{S,30}$ considered are shown in Fig. 6. The same layout as that presented in Fig. 5 is used. The left plot shows the results corresponding to the lateral KI factor and the right one those corresponding to the rotational KI factor. It can be observed that in the first mode and for the three types of soil profiles considered, the two KI factors remain practically constant as the $V_{S,30}$ of the soil increases. However, in the second mode, these two factors significantly change: the trend of the lateral KI factor is upward until a $V_{S,30}$ of approximately 150 m/s, then, from this speed, this factor remains practically constant; the trend of the rotational KI factor is generally decreasing as stiffness increases in all seabed profiles. Furthermore, if results are compared based on the types of soil profiles considered, it is observed that the rotational KI factors corresponding to the homogeneous soil profiles are the largest, followed by those obtained for the non-homogeneous with $n = 0.25$, revealing the influence that the non-homogeneity of the soil has on the pile head rotation, since the greater the stiffness in the deep layers, the smaller the rotation obtained. Besides, a common trend can be observed in the two KI factors for both modes,

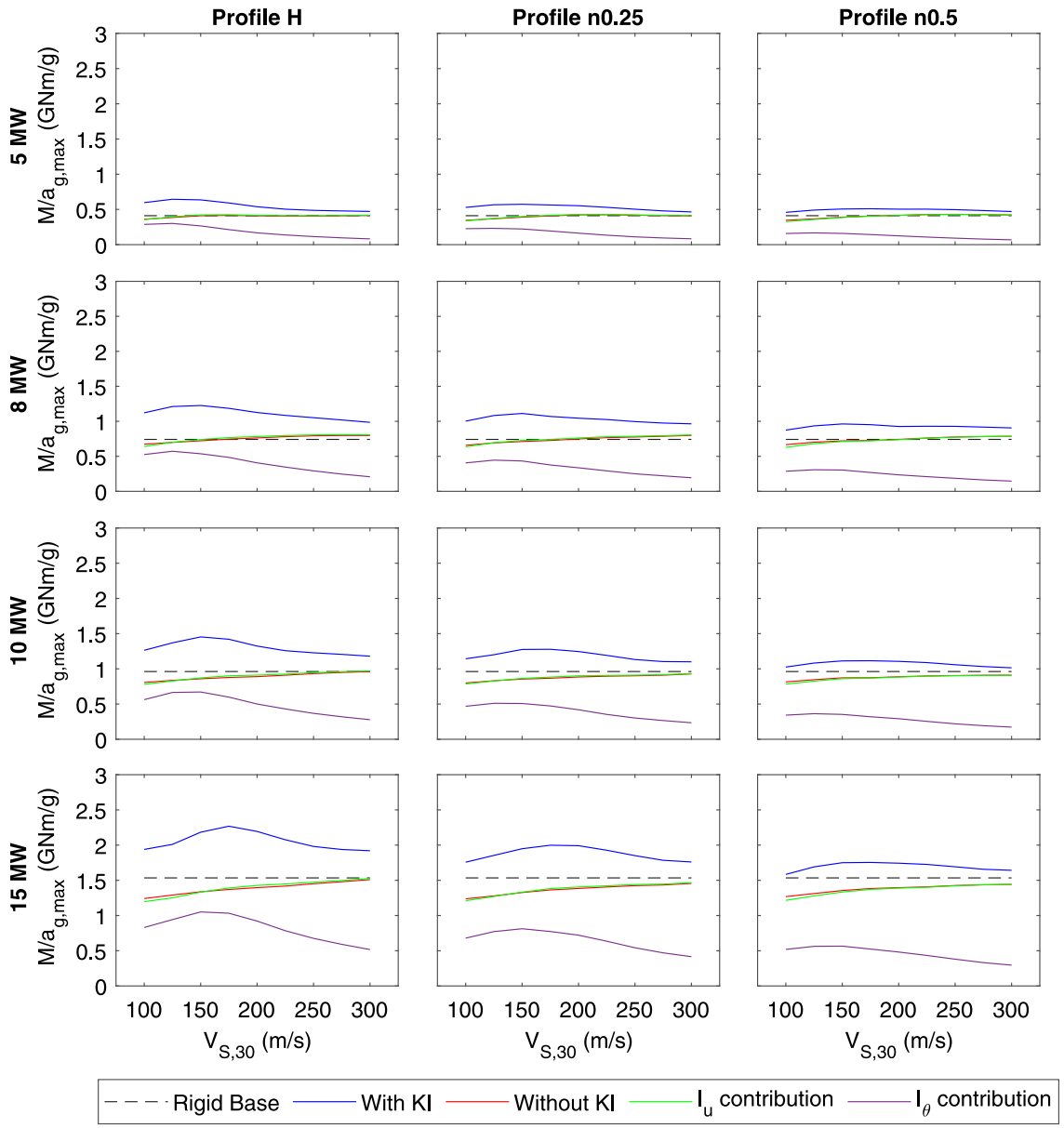

Fig. 9. Bending moments at the mudline level vs $V_{S,30}$ for all the study cases.

the KI factors computed for the three different profiles tend to each other as the value of $V_{S,30}$ increases, notice how the curves tend to approach each other. On the other hand, comparing the results that are obtained in the first mode with those of the second mode, it is observed that in the second mode the lateral KI factors corresponding to the homogeneous and those for the variable soil with $n = 0.25$ are slightly higher than those for the first mode, except for soil profiles with $V_{S,30}$ less than 150 m/s. The opposite occurs for the non-homogeneous profile with $n = 0.5$, where the lateral KI factors are greater in the first mode than in the second one. Finally, considering the rotational KI factor, higher results are reached in the second mode than in the first one for all soils.

4.2. Maximum seismic response

In order to quantify the influence of SSI and within this, the repercussion of each KI factor in the three types of soil profiles considered, the system maximum seismic response is studied for the four OWTs (shown in Table 1) and the different models considered (described in Section 2.3). This maximum response refers to the average obtained by taking into account all the seismic excitations (shown in Table 2). The system maximum response is studied in terms of maximum seismic bending moments and shear

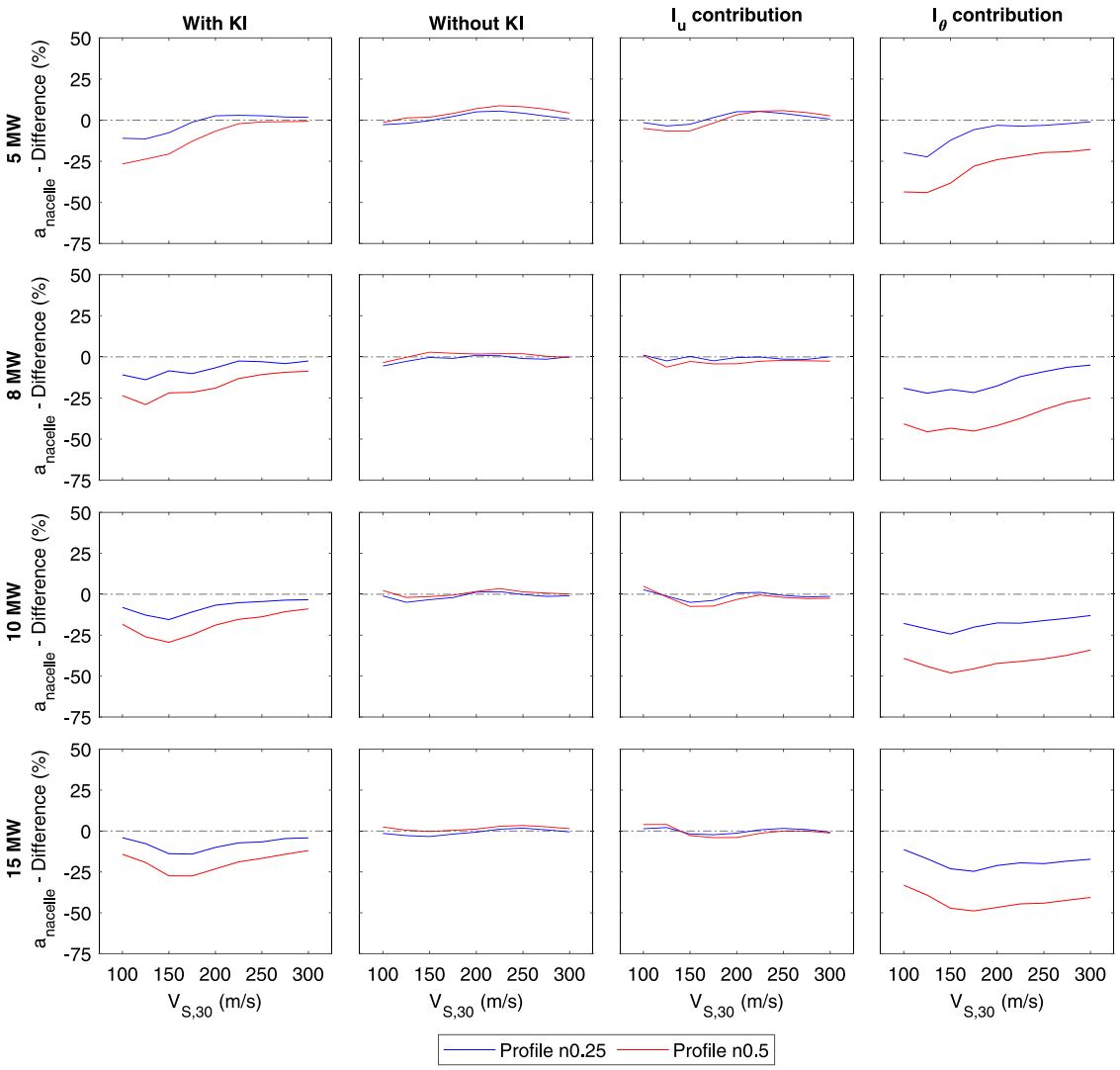

Fig. 10. Relative differences of the maximum amplification factors with respect to those of the homogeneous soil profile.

forces, which are computed at the mudline level, and in terms of relevant acceleration amplification factors at the nacelle height. The amplification factor is computed as the relation between the maximum acceleration of the nacelle and the maximum ground acceleration. Thus, this term quantifies how much the movement of the nacelle increases with respect to the free-field motion. Fig. 7 shows the amplification factors, while Figs. 8 and 9 display maximum shear forces and bending moments, respectively. These three figures show the results arranged in the same way, each figure is made up of different subgraphs, where the maximum scaled seismic response is represented against the different $V_{S,30}$ considered. The results of each wind turbine are arranged by rows while those corresponding to the different soil profiles are arranged by columns. Moreover, the results of each model considered are represented with different colours as indicated in the figure legend.

In all these representations, it is observed that the system greatest responses are obtained for the homogeneous soil profile. Note that this is mainly due to the influence of the rotational KI factor in the second mode of vibration, which is greater in the homogeneous soil profile (see Fig. 6). It can also be seen that as soil stiffness increases (crescent $V_{S,30}$), the results computed for the homogeneous and non-homogeneous with $n = 0.25$ profiles tend to coincide with each other (generally for $V_{S,30} \geq 200$ m/s). Note that this trend has also been obtained for the rotational KI factors around the second mode. In addition, it is observed that as the size of the wind turbine increases, greater shear forces and bending moments are reached in all seabed profiles. Nevertheless, in the amplification factors, the maximum values are obtained for the two smallest wind turbines. Also, analysing the results of the complete SSI model ("with KI"), in which the highest seismic responses are reached, it can be observed that as the size of the OWT increases, the system maximum response occurs for increasingly rigid soils (note how the highest value of the blue curve in Figs. 7–9 tends to move to the right).

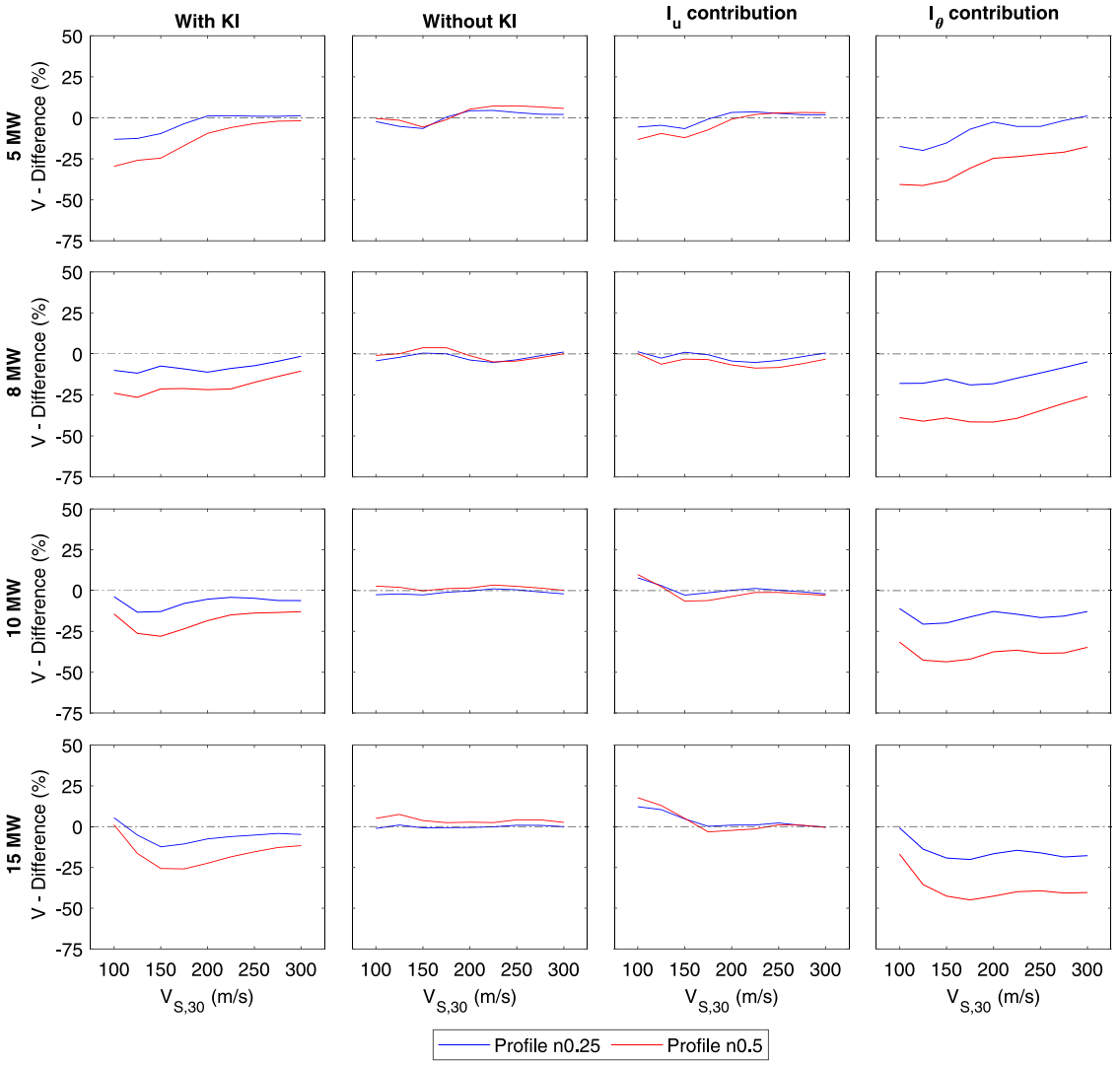

Fig. 11. Relative differences of the maximum shear forces with respect to those of the homogeneous soil profile.

On the other hand, when the influence of SSI is analysed, that is, comparing the blue curve (flexible base "with KI") with the black curve ("rigid base"), it can be observed that the system seismic response reached in the "with KI" model is greater than the response of the "rigid base" assumption, which reveals the influence that the consideration of SSI has on the seismic analysis.

Regarding the influence of KI, comparing the results corresponding to the "with KI" and "without KI" models (blue and red curve respectively), it can be seen the importance of considering the KI in the SSI, since remarkable greater responses are obtained in the "with KI" model. Moreover, it can be observed in all cases that results computed for the "without KI" and "I_u contribution" models are similar to each other, note the closeness between the green and red curves. This highlights the remarkable influence of the rotational KI factor on the seismic response of this type of structures, since the difference between considering or not the KI is marked by the "I_θ contribution" model. Note also the similarity in the shape of the curves in the "with KI" and "I_θ contribution" models. In addition, these two curves are quite similar to the curves of the rotational KI factors for the second vibration mode (previously shown in Fig. 6). This similarity is due to the fact that the effect of KI largely depends on the monopile rotation, which is greater in the second mode than in the first one (as confirmed by Kaynia [21]). Besides, it should be noticed that in the "with KI" and "I_θ contribution" models, the less pronounced the variation of the soil shear-wave velocity with depth and the larger the OWT, the greater the shear forces and bending moments.

4.3. Influence of the soil profile

With the aim of quantifying the relevance of considering a non-homogeneous profile with respect to a homogeneous one in the system seismic response, the results corresponding to the two variable profiles are compared against those computed for their

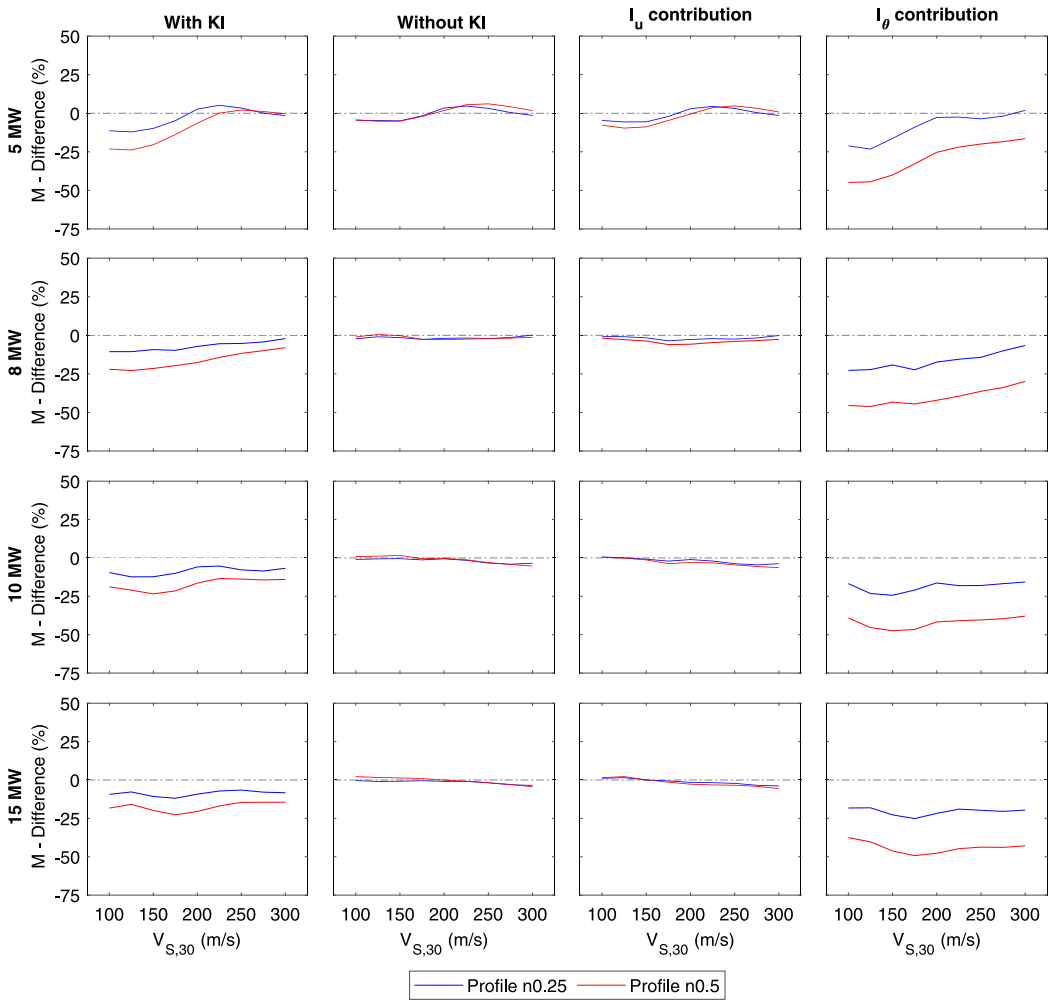

Fig. 12. Relative differences of the maximum bending moments with respect to those of the homogeneous soil profile.

equivalent homogeneous profile. For this purpose, the relative differences between the maximum results obtained in the two non-homogeneous profiles with respect to those corresponding to the homogeneous profile are studied. These relative differences in terms of maximum amplification factors, shear forces and bending moments for the different shear-wave velocities considered, are shown in Figs. 10, 11 and 12, respectively. Results for each OWT are arranged by rows, while results corresponding to different models are shown by columns. The two non-homogeneous profiles considered are depicted with a blue ($n = 0.25$) and a red ($n = 0.5$) curve respectively.

In all these representations it can be seen that the greatest differences arising from the soil profile occur when the rotational KI factor is considered ("with KI" and "I_θ contribution" models). Furthermore, these greater differences are obtained in soft soils ($V_{S,30}$ from 100 to 150 m/s), then, as soil stiffness increases, the differences tend to decrease. The greatest relative differences are found in the non-homogeneous profile with $n = 0.5$, doubling and even tripling those obtained for the non-homogeneous profile with $n = 0.25$. Note that the maximum differences in the "with KI" model are approximately 10% for the soil profile with $n = 0.25$, while in the profile with $n = 0.5$ they are between 25%–30%.

On the other hand, it is noteworthy that the differences arising from considering the non-homogeneity of the soil are due to the rotational KI factor. Note how the largest relative differences are those obtained with this model. While in the "without KI" and "I_u contribution" models, generally, the consideration of the non-homogeneity of the soil seems to be irrelevant, since the resulting differences in these two models are quite small. Nevertheless, for the two largest OWTs, remarkable differences are found in the "I_u contribution" model for soft soils, where differences reach approximately 20%, obtaining greater shear forces in the non-homogeneous profiles. Despite this fact, generally, for all the models, OWTs and $V_{S,30}$ considered, results corresponding to the $V_{S,30}$-equivalent homogeneous profile are greater than those corresponding to the variable profiles.

5. Conclusions

This paper studies the influence that the type of soil profile has on the seismic response of monopile-supported OWTs, including and analysing the inertial and kinematic interaction. For this purpose, three types of soil profiles are analysed, one homogeneous and two non-homogeneous (depth-dependent shear-wave velocity with semi-parabolic variation). Different values of time-average shear-wave velocity for the upper 30 m depth ($V_{S,30}$) are used for each of these three types of profiles, in order to analyse different soft-to-medium seabeds. Four references OWTs of different rated powers, with their corresponding monopiles, are considered. The system seismic response, in terms of maximum shear forces and bending moments at mudline level and acceleration amplification factors at hub level, is calculated using a finite element substructuring procedure. Several models that allow quantifying the influence of the inclusion of the inertial and kinematic interaction are used. The main conclusions drawn from the results are:

- Greater lateral impedances (K_H) are obtained for equivalent homogeneous soil profiles, but higher cross-coupled (K_{HR}) and rocking (K_R) impedances are reached for non-homogeneous seabed profiles. This effect is explained as the rotational motion is more affected by deeper ground properties than the lateral soil–pile motion.
- Related to the previous point, lower natural frequencies are reached for soils in which the variation of the shear-wave velocity with depth is more pronounced, indicating a major contribution of the lateral stiffness of the foundation.
- Regarding the KI factors, similar lateral KI factors (I_u) are obtained for the three soil profiles, while the rotational KI factor (I_θ) is more sensitive to soil profile type, obtaining higher rotational KI factors in the equivalent homogeneous profile.
- The highest seismic responses are obtained when both the inertial and kinematic soil–structure interaction are considered. Using a rigid base model or only incorporating the flexibility of the foundation leads to significantly smaller results than those obtained by the complete SSI model.
- However, the kinematic interaction only has a significant influence on the seismic response if the rotational KI factor is considered. This is directly related to the contribution of the second mode in the system response, as for the first mode the filtering effect of the foundation is negligible due to its low frequency.
- This influence of the rotational KI factor produces that, in general, greater seismic responses are obtained in the homogeneous seabed profile.
- Furthermore, the differences in the system seismic response owing to the definition of the soil profile are mainly explained by the rotational KI factor. These differences may be significant for soft soil profiles with pronounced variation of the shear-wave velocity with depth.

Declaration of competing interest

The authors declare that they have no known competing financial interests or personal relationships that could have appeared to influence the work reported in this paper.

Data availability

Data will be made available on request.

Acknowledgements

This research has been funded by Ministerio de Ciencia e Innovación and Agencia Estatal de Investigación (MCIN/AEI/10.13039/501100011033) of Spain and FEDER through research project PID2020-120102RBI00 and predoctoral research scholarship PRE2021-099200 (E. Rodríguez-Galván). This research was partially supported by ACIISI, Spain-Gobierno de Canarias and European FEDER Funds Grant EIS 2021 04.

References

[1] DNVSeismic Design of Wind Power Plants DNV-RP-0585; 2021. Det-Norske Veritas AS. 2022, Available online: https://www.dnv.com/energy/standards-guidelines/dnv-rp-0585-seismic-design-of-wind-power-plants.html. [Accessed on 24 august 2022].
[2] Medina C, Álamo GM, Quevedo-Reina R. Evolution of the seismic response of monopile-supported offshore wind turbines of increasing size from 5 to 15 MW including dynamic soil-structure interaction. J Mar Sci Eng 2021;9(11):1285.
[3] Padrón LA, Carbonari S, Dezi F, Morici M, Bordón JDR, Leoni G. Seismic response of large offshore wind turbines on monopile foundations including dynamic soil–structure interaction. Ocean Eng 2022;257:111653.
[4] Ju SH, Huang YC. Analyses of offshore wind turbine structures with soil-structure interaction under earthquakes. Ocean Eng 2019;187:106190.
[5] Wang W, Gao Z, Li X, Moan T. Model test and numerical analysis of a multi-pile offshore wind turbine under seismic, wind, wave, and current loads. J Offshore Mech Arct Eng 2017;139(3).
[6] Liang F, Yuan Z, Liang X, Zhang H. Seismic response of monopile-supported offshore wind turbines under combined wind, wave and hydrodynamic loads at scoured sites. Comput Geotech 2022;144:104640.
[7] Wang P, Zhao M, Du X, Liu J, Xu C. Wind, wave and earthquake responses of offshore wind turbine on monopile foundation in clay. Soil Dyn Earthq Eng 2018;113:47–57.
[8] Xi R, Xu C, Du X, El Naggar MH, Wang P, Liu L, et al. Framework for dynamic response analysis of monopile supported offshore wind turbine excited by combined wind-wave-earthquake loading. Ocean Eng 2022;247:110743.
[9] Patra SK, Haldar S. Seismic response of monopile supported offshore wind turbine in liquefiable soil. In: Structures, vol. 31. Elsevier; 2021, p. 248–65.

[10] Álamo GM, Aznárez JJ, Padrón LA, Martínez-Castro AE, Gallego R, Maeso O. Dynamic soil-structure interaction in offshore wind turbines on monopiles in layered seabed based on real data. Ocean Eng 2018;156:14–24.
[11] Shi S, Zhai E, Xu C, Iqbal K, Sun Y, Wang S. Influence of pile-soil interaction on dynamic properties and response of offshore wind turbine with monopile foundation in sand site. Appl Ocean Res 2022;126:103279.
[12] Arany L, Bhattacharya S, Macdonald JHG, Hogan SJ. Closed form solution of Eigen frequency of monopile supported offshore wind turbines in deeper waters incorporating stiffness of substructure and SSI. Soil Dyn Earthq Eng 2016;83:18–32.
[13] Yang Y, Bashir M, Li C, Wang J. Analysis of seismic behaviour of an offshore wind turbine with a flexible foundation. Ocean Eng 2019;178:215–28.
[14] Ghaemmaghami AR, Mercan O, Kianoush R. Seismic soil–structure interaction analysis of wind turbines in frequency domain. Wind Energy 2017;20(1):125–42.
[15] Mo R, Cao R, Liu M, Li M. Effect of ground motion directionality on seismic dynamic responses of monopile offshore wind turbines. Renew Energy 2021;175:179–99.
[16] Jiang W, Lin C. Lateral responses of monopile-supported offshore wind turbines in sands under combined effects of scour and earthquakes. Soil Dyn Earthq Eng 2022;155:107193.
[17] Jiang W, Lin C, Sun M. Seismic responses of monopile-supported offshore wind turbines in soft clays under scoured conditions. Soil Dyn Earthq Eng 2021;142:106549.
[18] De Risi R, Bhattacharya S, Goda K. Seismic performance assessment of monopile-supported offshore wind turbines using unscaled natural earthquake records. Soil Dyn Earthq Eng 2018;109:154–72.
[19] Bisoi S, Haldar S. Dynamic analysis of offshore wind turbine in clay considering soil-monopile-tower interaction. Soil Dyn Earthq Eng 2014;63:19–35.
[20] API RP 2A-WSDRecommended Practice for Planning, Designing and Constructing Fixed Offshore Plaftorms - Working Stress Design. American Petroleum Institute.
[21] Kaynia AM. Effect of kinematic interaction on seismic response of offshore wind turbines on monopiles. Earthq Eng Struct Dyn 2021;50(3):777–90.
[22] Wind Europe. Offshore wind in Europe – Key trends and statistics 2020. Technical report, Brussels, Belgium: WindEurope asbl/vzw; 2021.
[23] Álamo GM, Martínez-Castro AE, Padrón LA, Aznárez JJ, Gallego R, Maeso O. Efficient numerical model for the computation of impedance functions of inclined pile groups in layered soils. Eng Struct 2016;126:379–90.
[24] Chopra AK. Dynamics of structures. Theory and applications to earthquake engineering. Seventh ed. NJ, USA: Pearson/Prentice Hall, Englewood Cliffs; 2017.
[25] Álamo GM, Bordón JDR, Aznárez JJ. On the application of the beam model for linear dynamic analysis of pile and suction caisson foundations for offshore wind turbines. Comput Geotech 2021;134:104107.
[26] Arany L, Bhattacharya S, Macdonald J, Hogan SJ. Design of monopiles for offshore wind turbines in 10 steps. Soil Dyn Earthq Eng 2017;92:126–52.
[27] Jonkman J, Butterfield S, Musial W, Scott G. Definition of a 5-MW reference wind turbine for offshore system development. Technical report, Golden, CO (United States): National Renewable Energy Lab.(NREL); 2009.
[28] Desmond C, Murphy J, Blonk L, Haans W. Description of an 8 MW reference wind turbine. In: Journal of physics: Conference series, vol. 753, no. 9. IOP Publishing; 2016, 092013.
[29] Bak C, Zahle F, Bitsche R, Kim T, Yde A, Henriksen LC, et al. The DTU 10-MW reference wind turbine. In: Danish wind power research 2013. 2013.
[30] Gaertner E, Rinker J, Sethuraman L, Zahle F, Anderson B, Barter G, et al. Definition of the IEA 15-Megawatt offshore reference wind turbine. National Renewable Energy Laboratory (NREL); 2020.
[31] Wang SY, Wang HY. Site-dependent shear-wave velocity equations versus depth in California and Japan. Soil Dyn Earthq Eng 2016;88:8–14.
[32] Hamilton EL. Shear-wave velocity versus depth in marine sediments: A review. Log Anal 1977;18(01).
[33] European Committee for Standardization. Eurocode 8: Design of structures for earthquake resistance. Part 5: Foundations, Retaining Structures and Geotechnical Aspects. 2004, Brussels.
[34] Pacific Earthquake Engineering Research Center (PEER). NGA-West2 Ground Motion Database. 2022, Available online: . [Accessed on 20 august 2022].
[35] Kaynia AM, Kausel E. Dynamics of piles and pile groups in layered soil media. Soil Dyn Earthq Eng 1991;10(8):386–401.
[36] Miura K, Kaynia AM, Masuda K, Kitamura E, Seto Y. Dynamic behaviour of pile foundations in homogeneous and non-homogeneous media. Earthq Eng Struct Dyn 1994;23(2):183–92.
[37] Álamo GM, Martínez-Castro AE, Padrón LA, Aznárez JJ, Gallego R, Maeso O. A proposal for normalized impedance functions of inclined piles in non-homogeneous media. Procedia Eng 2017;199:86–91.